Amide proton transfer-weighted imaging combined with multiple models diffusion-weighted imaging of endometrial cancer: correlations between multi-modal MRI parameters and HIF-1α expression

Jun Li[1], Changjun Ma[2], Shifeng Tian[1,3], Ailian Liu[1,3,4*],
Qingling Song[1,3], Nan Wang[1,3], Qingwei Song[1,3], Liangjie Lin[5],
Peng Sun[5] and Jiazheng Wang[5]

[1]Department of Radiology, The First Affiliated Hospital of Dalian Medical University, Dalian,
Liaoning, China, [2]School of Biomedical Engineering, Faculty of Medicine, Dalian University of
Technology, Dalian, Liaoning, China, [3]Dalian Medical Image Artificial Intelligence Engineering
Technology Research Center, Dalian, Liaoning, China, [4]Technology Innovation Center of
Hyperpolarized MRI, Dalian, Liaoning, China, [5]Philips Health Technology (China) Co., Ltd.,
Beijing, China

Background: Hypoxia inducible factor (HIF-1α) is a major transcriptional factor regulating gene expression under hypoxic conditions. HIF-1α expression was closely correlated with the oxygenation status of tumor and could serve as an important biomarker for tumor hypoxia, aggressiveness, or radiation resistance. High expression of HIF-1α contributes to high aggressiveness or poor prognosis of endometrial cancer.

Purpose: This study aimed to investigate correlations between multimodal MRI parameters (derived from amide proton transfer weighted imaging [APTw], conventional diffusion weighted imaging [DWI], intravoxel incoherent motion [IVIM] imaging and diffusion kurtosis imaging [DKI]) and HIF-1α expression, and to determine whether multimodal MRI can be used for quantitative evaluation of HIF-1α expression.

Study type: Retrospective.

Population: A total of 94 patients with EC were examined with 32 cases finally included in the high HIF-1α expression group and 40 cases included in the low expression group according to the exclusion and inclusion criteria.

Field Strength/Sequence: 3.0T/APTw, DWI, IVIM, and DKI

Assessment: The asymmetry of magnetization transfer rate (MTR$_{asym}$), apparent diffusion coefficient (ADC), pure diffusion coefficient (D), pseudo diffusion coefficient (D*), perfusion fraction (f), mean kurtosis (MK), and mean diffusivity (MD) were calculated from multimodal MRI and compared between HIF-1α high expression and HIF-1α low expression groups.

Statistical Test: Mann–Whitney U-test; Chi-square test or Fisher exact test; logistic regression analysis; Area under the receiver operating characteristic (ROC) curve (AUC); The Delong test; Pearson or Spearman correlation coefficients. The significance threshold was set at $P < 0.05$.

Result: MTR_{asym}, ADC, D, D*, MK and MD values were significantly higher in high HIF-1α expression than in low HIF-1α expression groups, whereas f value was significantly lower in high HIF-1α expression than in low HIF-1α expression groups. The AUC of HIF-1 α expression evaluated by MTR_{asym}, ADC, D, D*, f, MD, MK and their combination were 0.894 (0.740, 0.973), 0.746 (0.568, 0.879), 0.716 (0.528, 0.904), 0.920 (0.772, 0.984), 0.756 (0.578, 0.886), and 0.973 (0.851-1.000), respectively. Multivariate analysis revealed that only f, MK, and MD values were independent predictors for evaluating HIF-1α expression in EC.

Conclusion: APTw combined with multi-model diffusion imaging can quantitatively evaluate the expression of HIF-1α in EC, and the combination of multiple quantitative parameters can improve the evaluation efficiency.

Introduction

Endometrial cancer (EC) is a neoplasm that arises from the endometrium and is the second most prevalent malignancy affecting the female reproductive system in China (1, 2). It is the most frequently diagnosed gynecological tumor in developed nations, with a steadily increasing incidence (3). Approximately 70% of EC cases are localized to the uterine body, representing an early clinical stage with a favorable prognosis (4). Surgery intervention is the primary treatment for EC, with radiotherapy, chemotherapy, and hormone therapy often used as adjuvant therapies. tumors are divided into four subgroups: polymerase-epsilon (POLE) mut,

---

Abbreviations: MRI, Magnetic resonance imaging; EC, Endometrial cancer; APT, Amide proton transfer; MTR_{asym}, Asymmetric magnetization transfer rate; IVIM, Intravoxel incoherent motion; DKI, Diffusion kurtos imaging; HIF-1α, Human epidermal growth factor receptor-2; CEST, Chemical exchange saturation transfer; ROI, Regions of interest; ICC, Intra-group correlation coefficient; ROC, Receiver operating characteristic; AUC, Area under the curve; IHC, Immunohistochemistry; FISH, Fluorescence *in situ* hybridization; VEGF, Vascular endothelial growth factor; APTw, Amide proton transfer weighting; DKI, Diffusion kurtosis imaging; IVIM, Intravoxel incoherent motion; HIF-1α, Human epidermal growth factor receptor-2; T_2WI, T2-weighted Imaging; ADC, Apparent diffusion coefficient; DWI, Diffusion-weighted imaging; D, pure diffusion coefficient; D*, pseudo diffusion coefficient; f, perfusion fraction; FA, fractional anisotropy; MK, mean kurtosis; MD, mean diffusivity; HIF-1α, Human epidermal growth factor receptor-2; MTR_{asym}, Asymmetric magnetization transfer rate; MTR_{asym}, Asymmetric magnetization transfer rate; EC, endometrial cancer.

protein 53 (p53) wild type, p53 missense mutations and mismatch repair deficient (5). In the face of such a complex disease classification, when choosing the treatment of endometrial cancer, we should consider the patient's age, pathological type, molecular classification and clinical stage (low, medium, high risk) and other factors, in order to optimize the outcome of patients (6). Typically, patients with stage I and stage II endometrial cancer with localized tumors opt for hysterectomy in the absence of high-risk factors. Conversely, patients with high-risk factors, such as extrauterine metastasis, may benefit from concurrent radiotherapy and chemotherapy to enhance treatment efficacy (7, 8). Progesterone therapy is typically recommended as the initial treatment for EC patients seeking to preserve their fertility (9). At the same time, systematic assessment, such as microsatellite instability, has been practiced and applied in clinical practice. For patients with this specific biomarker, Programmed Death-1/Programmed Death-Ligand 1 inhibitors have shown promising therapeutic outcomes (10). Radiotherapy plays a crucial role in the treatment of advanced stage EC patients with high-risk features, such as extrauterine invasion, although individual responses to this treatment may vary. Numerous variables influence the efficacy of radiotherapy, including cellular processes such as growth and apoptosis, the presence of a hypoxic microenvironment, angiogenesis, and temperature. Among these factors, hypoxia inducible factor (HIF-1α) is specifically associated with the hypoxic microenvironment (11, 12).

HIF-1α serves as a key transcription factor that regulates gene expression under hypoxia (13–15). Prior studies have shown that (14, 16, 17) the expression of HIF-1α is closely related to the oxygenation state of the tumor. In normoxic conditions, HIF-1α undergoes rapid

degradation, whereas in hypoxic environments, the degradation of HIF-1α is inhibited, leading to its accumulation in the nucleus. This phenomenon can serve as a significant biomarker for tumor hypoxia, invasiveness, and resistance to radiation therapy (18). Additionally, HIF-1α plays a crucial role in regulating various cellular functions in response to low oxygen levels, including glucose uptake, energy metabolism, angiogenesis, erythropoiesis, cell proliferation, apoptosis, cell-cell and cell-matrix interactions, which collectively contribute to processes such as tumorigenesis, metastasis, and epithelial-mesenchymal transformation (EMT) (19, 20). Conversely, elevated levels of HIF-1α can impact the efficacy of tumor therapy by modulating downstream and upstream molecular signaling pathways and influencing the expression of hypoxia-related genes involved in angiogenesis, erythropoiesis, glycolysis, cell adhesion, cell proliferation, and apoptosis (21), meanwhile, causing inadequate arterial blood supply, reduced vascular density, impaired vascular tissue transport efficiency, alterations in red blood cell flow, functional shunting, and imbalance of oxygen supply and demand (22). These effects ultimately contribute to tumor hypoxia and heightened invasiveness of endothelial cells, leading to an unfavorable prognosis for patients with EC and impacting treatment outcomes. Generally speaking (23), in the context of tumor hypoxia, the efficacy of tumor

radiotherapy and chemotherapy is typically diminished, necessitating the assessment of tumor hypoxia status to inform clinical interventions. Through an understanding of the molecular pathways involving HIF-1α, novel therapeutic approaches targeting highly expressed HIF-1α signaling pathways have been devised to enhance personalized and precise treatment for cancer patients (24, 25).

Previously, the identification of tumor molecules relied on invasive surgical procedures or biopsies to obtain tissue samples. However, the presence of tumor heterogeneity posed a challenge to the efficacy of these samples, as small tissue samples were unable to accurately represent the entire tumor (26). In addition, although impact genomics has been used in molecular/genome analysis, it is hindered by the widespread use of factors such as technical complexity (27, 28). Previous methods for assessing tumor hypoxia included direct approaches such as the use of oxygen sensing probes (29) and phosphorescence lifetime imaging to measure PO_2 (30), as well as indirect methods like oxygen-enhanced magnetic resonance imaging (OE-MRI) (31), magnetic susceptibility imaging (19), and positron emission tomography (PET) (32) to infer tumor hypoxia. At the same time, some studies have also found that there is a correlation of the quantitative parameters measured by dynamic contract-enhanced magnetic resonance imaging (DCE-MRI) (33), diffusion weighted
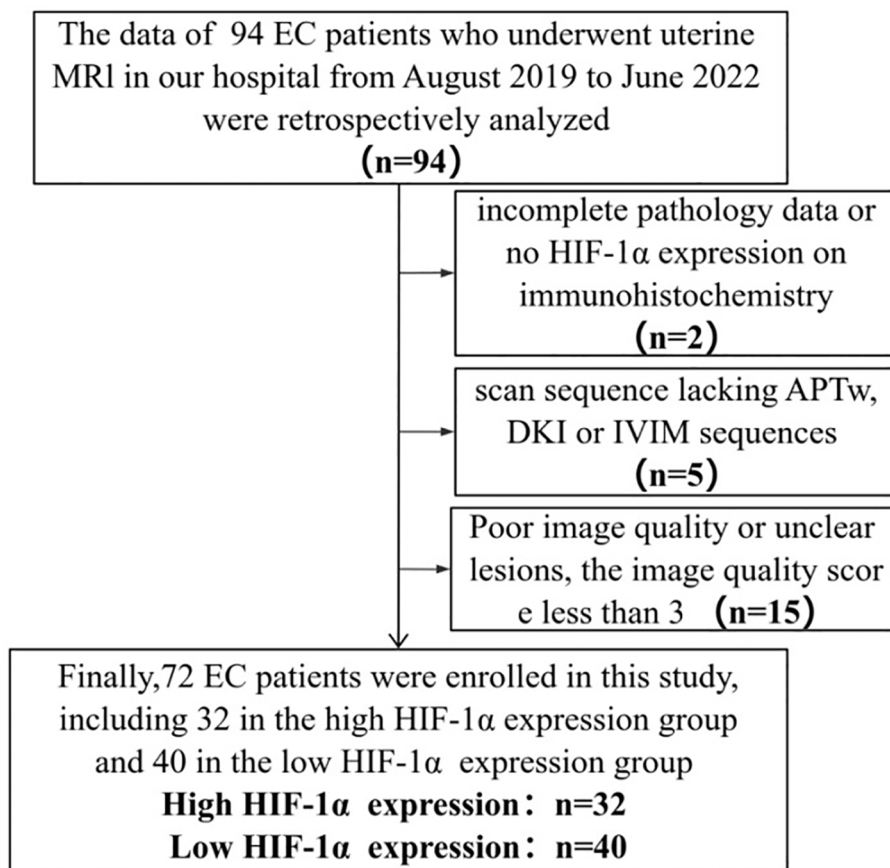

FIGURE 1
Flow chart of patient enrollment.

imaging (DWI) (34) and intravoxel incoherent motion (IVIM) (35) with tumor hypoxia. Among all these imaging parameters, no individual one can serve as a definitive marker for assessing tumor oxygenation. Conversely, the utilization of multiple imaging parameters obtained through multi-parameter imaging technology is anticipated to have a greater impact on the assessment of tumor hypoxia. Thus, this study employed a combination of amide proton transfer weighted imaging (APTw), DWI, IVIM, and diffusion kurtosis imaging (DKI) to examine the expression of EC HIF-1α in relation to tumor metabolism and blood perfusion.

Materials and methods

Study population

The Ethics Committee approved the retrospective study and waived the requirement for informed consent. The retrospective analysis examined the clinical and imaging data of 94 patients who underwent 3.0T MR examination at our hospital between August 2019 and June 2022, and were subsequently diagnosed with EC following uterine curettage or pathology. Inclusion criteria for the study

TABLE 1 Patient characteristics.

	n	High HIF-1α expression n=32	Low HIF-1α expression n=40	χ^2/t	P
Age (y)[1]	72	59.44 ± 10.15	58.25 ± 9.18	0.520	0.604
FIGO Stage n (%)					
Stage I	52	24/32 (75.00)	28/40 (70.00)	3.275	0.333
Stage II	6	4/32 (12.50)	2/40 (5.00)		
Stage III	12	3/32 (9.38)	9/40 (22.50)		
Stage IV	2	1/32 (3.12)	1/40 (2.50)		
Differentiation degree n (%)					
Low	26	15/32 (46.88)	11/40 (27.50)	4.011	0.136
Medium	34	11/32 (34.38)	23/40 (57.50)		
High	12	6/32 (18.75)	6/40 (15.00)		
Menopausal state n (%)					
Before	14	7/32 (21.88)	7/40 (17.50)	0.217	0.767
After	58	25/32 (78.13)	33/40 (82.50)		
Pathological type n (%)					
Type I	23	11/32 (34.38)	12/40 (30.00)	0.157	0.801
Type II	49	21/32 (65.63)	28/40 (70.00)		
Irregular vaginal bleeding n (%)					
No	43	15/32 (46.88)	28/40 (70.00)	3.952	***0.040***
Yes	29	17/32 (53.12)	12/40 (30.00)		
DMI n (%)					
<1/2 muscular layer	19	11/32 (34.38)	8/40 (20.00)	1.891	0.189
≥1/2 muscular layer	53	21/32 (65.62)	32/40 (80.00)		
LVSI n (%)					
Positive	14	7/32 (21.88)	7/40 (17.50)	0.217	0.767
Negative	58	25/32 (78.12)	33/40 (82.50)		
LNM n (%)					
Positive	11	3/32 (9.38)	8/40 (20.00)	1.551	0.325
Negative	61	29/32 (90.62)	32/40 (80.00)		

HIF-1α, hypoxia inducible factor; FIGO, Federation International of Gynecology and Obstetr; DMI, deep myometrium invasion; LVSI, Lymph-vascular space invasion; LNM, lymph node metastasis.
The bold values in the tables indicate p-values < 0.05, denoting statistical significance.

TABLE 2 Main imaging parameters of the MRI sequences.

Series	Orientation	TR/TE (ms)	FOV (mm³)	ACQ Voxel (mm³)	Thickness/Gap(mm)	Slices	Scan Time (Min sec)
T$_2$WI	TRA	4596/95	240 × 240 × 99	0.7 × 0.7 × 4.0	4.0/1.0	20	1 min 14 s
T$_2$WI	SAG	4930/84	250 × 250 × 99	0.95 × 0.95 × 4.0	4.0/1.0	20	2 min 08 s
DWI	COR	7800/72	380 × 380 × 105	3.0 × 3.0 × 3.0	3.0/0	35	3 min 31 s
IVIM	SAG	2500/94	380 × 380 × 65	3.0 × 3.0 × 5.0	5.0/1.0	11	5 min 23 s
DKI	SAG	1997/89	380 × 356 × 95	3.0 × 3.0 × 5.0	5.0/1.0	16	5 min 29 s
APTw	SAG	6416/7.8	130 × 130 × 49	2.0 × 2.0 × 7.0	7.0/0	7	5 min 53 s

TR, repetition time; TE, echo time; FOV, Field of View; ACQ, Acquisition; T2WI, T2-weighted Imaging; DWI, Diffusion-Weighted Imaging; IVIM, Intravoxel Incoherent Motion; DKI, Diffusion Kurtosis Imaging; APTw, Amide Proton Transfer weighting; TRA, Transverse; SAG, Sagittal; COR, Coronal.

encompassed the presence of high-quality MRI images with clearly delineated lesions devoid of artifacts, facilitating the accurate identification of tumor boundaries during region of interest (ROI) delineation. Additionally, the inclusion criteria stipulated the presence of a solitary tumor without concurrent tumors or endometrial hyperplasia, as well as the absence of prior treatment for endometrial carcinoma prior to MRI examination. Exclusion criteria encompassed the absence of essential scan sequences such as APTw, DWI, IVIM, and DKI, suboptimal MRI image quality resulting in indistinct lesion visualization or tumor size less than 1cm, and incomplete clinicopathological data including the lack of HIF-1α expression

information. The flow chart of the incoming and outgoing group is shown in Figure 1. Finally, 72 patients were enrolled in this study. According to the expression of HIF-1α, they were divided into two groups: high expression of HIF-1α (n = 32) and low expression of HIF-1α (n = 40). The general clinicopathological data of the two groups of patients were collected through our hospital information management system, including age, differentiation degree, menopausal state, Federation International of Gynecology and Obstetr (FIGO) staging, deep myometrium invasion (DMI), lymph-vascular space invasion (LVSI), lymph node metastasis (LNM), and pathological type, as shown in Table 1.
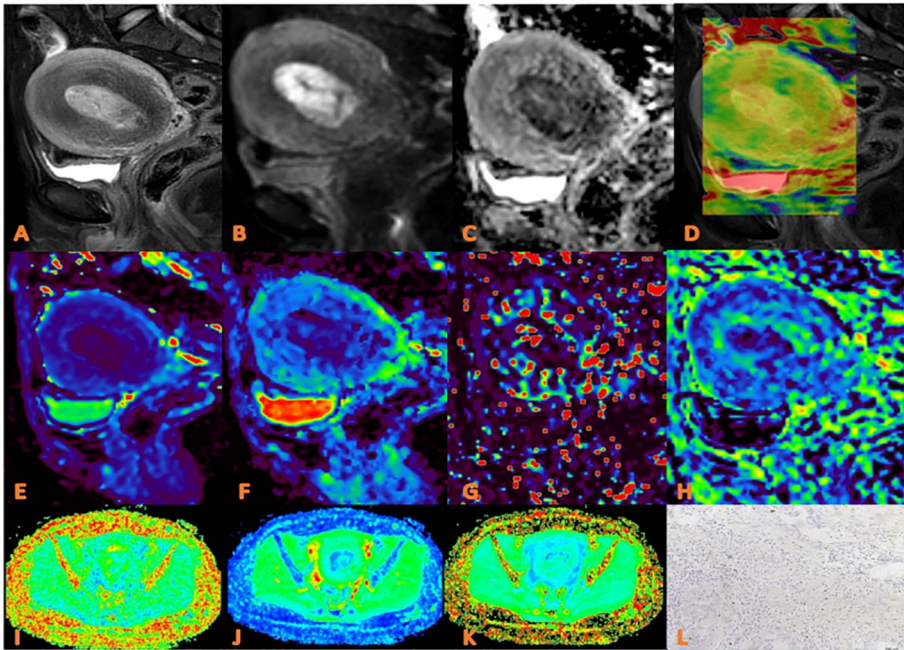
FIGURE 2
APTw, DKI and IVIM parameters for an EC patient with low HIF-1α expression. **(A)** sagittal T2WI, showing a slightly high signal mass in the uterine cavity; **(B)** sagittal DWI image; **(C)** sagittal ADC image; **(D)** APTw fused with T2WI (mean MTRasym value 2.90%) **(E−H)** ADC, D, D*, and f images. Mean values are 0.750 ×10-3 mm2/sec for ADC, 0.470 × 10-3 mm2/sec for D, 0.560×10-2 mm2 /sec for D* and 0.30% for f; **(I−K)** FA, MK, and MD images. Mean values are 0.314 for FA, 0.555 for MK, and 0.876 μm2/ms for MD; **(L)** Immunohistochemical staining image (×200) showed that HIF-1α expression of the tumor appeared as low expression.
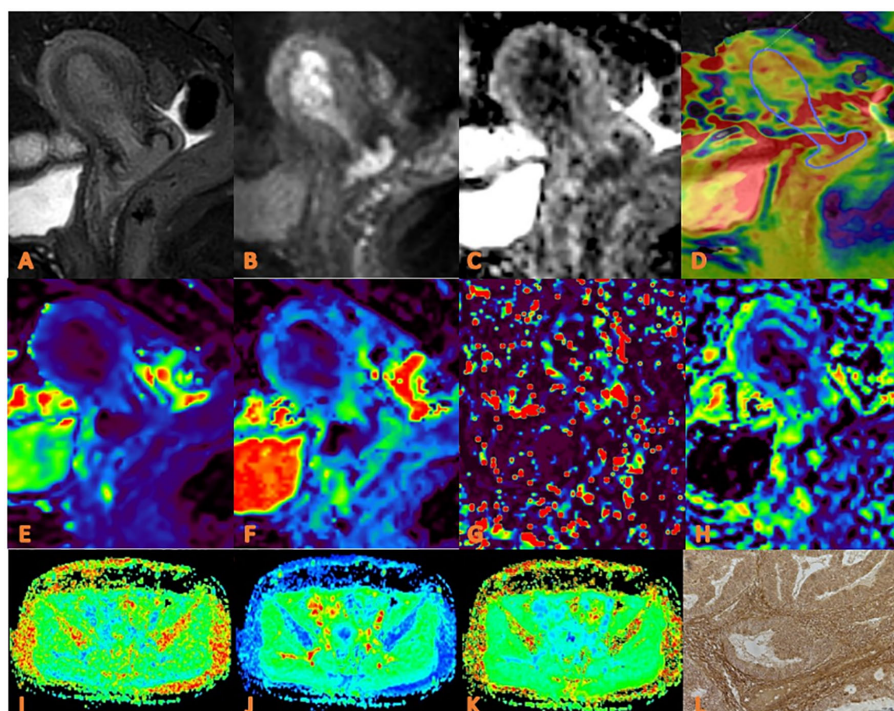
FIGURE 3
APTw, DKI and IVIM in EC that had high HIF-1α expression. **(A)** sagittal T2WI, showing a slightly high signal mass in the uterine cavity; **(B)** sagittal DWI image; **(C)** sagittal ADC images; **(D)** APTw and T2WI fusion images (mean APT value 3.07%) **(E–H)** ADC, D, D*, and f images. Mean values are 0.760×10⁻³ mm²/sec for ADC, 0.590 × 10⁻³ mm²/sec for D, 0.600 ×10⁻² mm²/sec for D* and 0.160% for f; **(I–K)** FA, MK, and MD images. Mean values are 0.395 for FA, 0.674 for MK, and 0.866μm² /ms for MD; **(L)** Immuno-histochemical staining image (×200) showed that HIF-1α expression of the tumor appeared as high expression.

MRI technique

MR scans were performed on a 3.0T MR scanner (Ingenia CX, Philips Healthcare, Best, the Netherlands) with a 32-channel abdominal coil. Before the examination, the patient was instructed to empty the bladder, and the intrauterine device was taken out one day before the examination. The patient was in the supine position with the feet advanced. The MRI sequences included transverse T2-weighted imaging (T2WI), sagittal T2WI, diffusion-weighted imaging (DWI) (b=0, 800 s/mm²), APTw, DKI (3 b values: 0, 1000, 2000 s/mm² and diffusion gradients were applied in 32 orthogonal directions) and IVIM (10 b values: 0, 20, 50, 100, 150, 200, 400, 800, 1200, 2000 s/mm²), and the specific parameters are shown in Table 2.

IVIM imaging evaluates the diffusion motion component and blood perfusion component separately through modelling of related quantitative parameters on the diffusion weighted images. The relationship between the signal change and all b-values can be expressed by the following equation (36).

$$S_b/S_0 = (1 - f) \cdot \exp(-bD) + f \cdot \exp[-b(D* + D)],$$

where b is the diffusion sensitivity factor, S_0 and S_b represent the signal intensities of b=0 s/mm² and all other b values, respectively. The f value is the perfusion fraction (between 0 and 1), which represents the volume ratio of the microcirculation perfusion in the voxel to the overall diffusion effect; the D value is the pure diffusion coefficient, which represents the pure water molecule diffusion

movement motion component; D* is the pseudo diffusion coefficient produced by blood circulation, which represents the incoherent motion of the microcirculation in the voxel; that is, the rapid diffusion motion related to perfusion. The IVIM data were processed on the Intellispace Portal v10.0 workstation (Philips Healthcare) using the advanced diffusion analysis tool.

APTw imaging was performed using a 3-dimensional (3D) turbo-spin-echo sequence with chemical shift-selective fat suppression. The middle slice of APTw images was located through the largest cross-section of the selected tumor lesion present on conventional MR images. Data were acquired with seven saturation-frequency offsets (± 2.7, ± 3.5, ± 4.3, and -1,540 ppm) for fitting of the Z-spectrum. Saturation radio-frequency pulses for APTw imaging were implemented with an amplitude of 2μT and a duration of 2 s. The acquisition was repeated three times at +3.5 ppm with shifted echo times for generation of B0 maps. B0-corrected ATPw images were reconstructed online. The MTR_{asym} (magnetization transfer ratio asymmetry) value at the frequency offset of +3.5 ppm was calculated as percent level (relative to S_0) for APTw quantitative analysis:

$$MTR_{asym}(3.5 \text{ ppm}) \times 100\%$$
$$= (S_{sat}(-3.5 \text{ ppm})/S_0 - S_{sat}(+3.5 \text{ ppm})/S_0)) \times 100\%$$

where S_0 is the water signal strength at a saturation frequency of -1540 ppm, and S_{sat} is the water signal strength at a saturation frequency of +3.5/-3.5 ppm after B0 correction.

TABLE 3 Inter-observer agreement on the measurement of imaging parameters.

Parameters	Number	Observer1	Observer2	Observer3	ICC
MTR_{asym} (%)	Low HIF-1α expression(n=40)	2.67 ± 0.90	2.77 ± 0.86	2.76 ± 0.86	0.923
	High HIF-1α expression(n=32)	3.19 ± 0.86	3.22 ± 0.87	3.17 ± 0.85	0.992
ADC ($\times 10^{-3}$mm^2/s)	Low HIF-1α expression(n=40)	0.678 ± 0.19	0.682 ± 0.19	0.684 ± 0.19	0.983
	High HIF-1α expression(n=32)	0.86 ± 0.28	0.87 ± 0.29	0.87 ± 0.30	0.997
D ($\times 10^{-3}$mm^2/s)	Low HIF-1α expression(n=40)	0.49 ± 0.13	0.49 ± 0.12	0.49 ± 0.12	0.968
	High HIF-1α expression(n=32)	0.70 ± 0.28	0.71 ± 0.28	0.71 ± 0.28	0.998
D* ($\times 10^{-2}$mm^2/s)	Low HIF-1α expression(n=40)	0.52 ± 0.29	0.53 ± 0.30	0.54 ± 0.29	0.991
	High HIF-1α expression(n=32)	2.45 ± 2.98	2.29 ± 2.87	2.26 ± 2.83	0.969
f (%)	Low HIF-1α expression(n=40)	0.40 ± 0.14	0.40 ± 0.16	0.40 ± 0.16	0.938
	High HIF-1α expression(n=32)	0.23 ± 0.18	0.24 ± 0.19	0.24 ± 0.17	0.991
MK	Low HIF-1α expression(n=40)	0.60 ± 0.11	0.60 ± 0.11	0.60 ± 0.10	0.998
	High HIF-1α expression(n=32)	0.70 ± 0.12	0.71 ± 0.12	0.71 ± 0.12	0.998
MD (μm^2/ms)	Low HIF-1α expression(n=40)	0.96 ± 0.19	0.95 ± 0.19	0.95 ± 0.19	0.995
	High HIF-1α expression(n=32)	1.20 ± 0.51	1.21 ± 0.54	1.21 ± 0.51	0.997
FA	Low HIF-1α expression(n=40)	0.33 ± 0.12	0.34 ± 0.12	0.34 ± 0.12	0.998
	High HIF-1α expression(n=32)	0.33 ± 0.11	0.33 ± 0.11	0.33 ± 0.10	0.999

ICC, Intra-group correlation coefficient; MTRasym, asymmetric magnetization transfer rate; ADC,Apparent diffusion coefficient; D, pure diffusion coefficient; D*, pseudo diffusion coefficient; f, perfusion fraction; MK, mean kurtosis; MD, mean diffusivity; FA, fractional anisotropy.

DKI uses 3 b values (0, 1000, and 2000 s/mm^2) and 32 orthogonal directions to obtain DKI parameters of fractional anisotropy (FA), mean kurtosis (MK) and mean diffusivity (MD) by the following equation (37):

$$S(b) = S(0) \cdot \exp(-b \cdot MD + 1/6 \cdot b^2 \cdot MD^2 \cdot MK)$$

where S(0) is the DWI signal of bounded 0, and S(b) is the DWI signal of a specific b value. MD represents the average diffusion

TABLE 4 Comparison of imaging parameters between low HIF-1α expression and high HIF-1α expression patient groups.

Parameters	High HIF-1α expression n=32	Low HIF-1α expression n=40	t/z	P
MTR_{asym} (%)	3.19 ± 0.85	2.73 ± 0.85	2.126	*0.034*
ADC ($\times 10^{-3}$mm^2/s)	0.87 ± 0.29	0.68 ± 0.19	3.038	*0.002*
D ($\times 10^{-3}$mm^2/s)	0.71 ± 0.28	0.49 ± 0.12	3.810	*<0.001*
D* ($\times 10^{-2}$mm^2/s)	2.34 ± 2.81	0.53 ± 0.29	4.145	*<0.001*
f (%)	0.24 ± 0.18	0.40 ± 0.15	-4.757	*<0.001*
MK	0.708 ± 0.118	0.602 ± 0.108	3.621	*<0.001*
MD (μm^2/ms)	1.207 ± 0.517	0.961 ± 0.190	1.989	*0.047*
FA	0.334 ± 0.107	0.339 ± 0.121	0.011	0.991

HIF-1α, Human epidermal growth factor receptor-2; MTRasym, Asymmetric magnetization transfer rate; ADC, Apparent diffusion coefficient; D, pure diffusion coefficient; D*, pseudo diffusion coefficient; f, perfusion fraction; MK, mean kurtosis; MD, mean diffusivity; FA, fractional anisotropy.
The bold values in the tables indicate p-values < 0.05, denoting statistical significance.
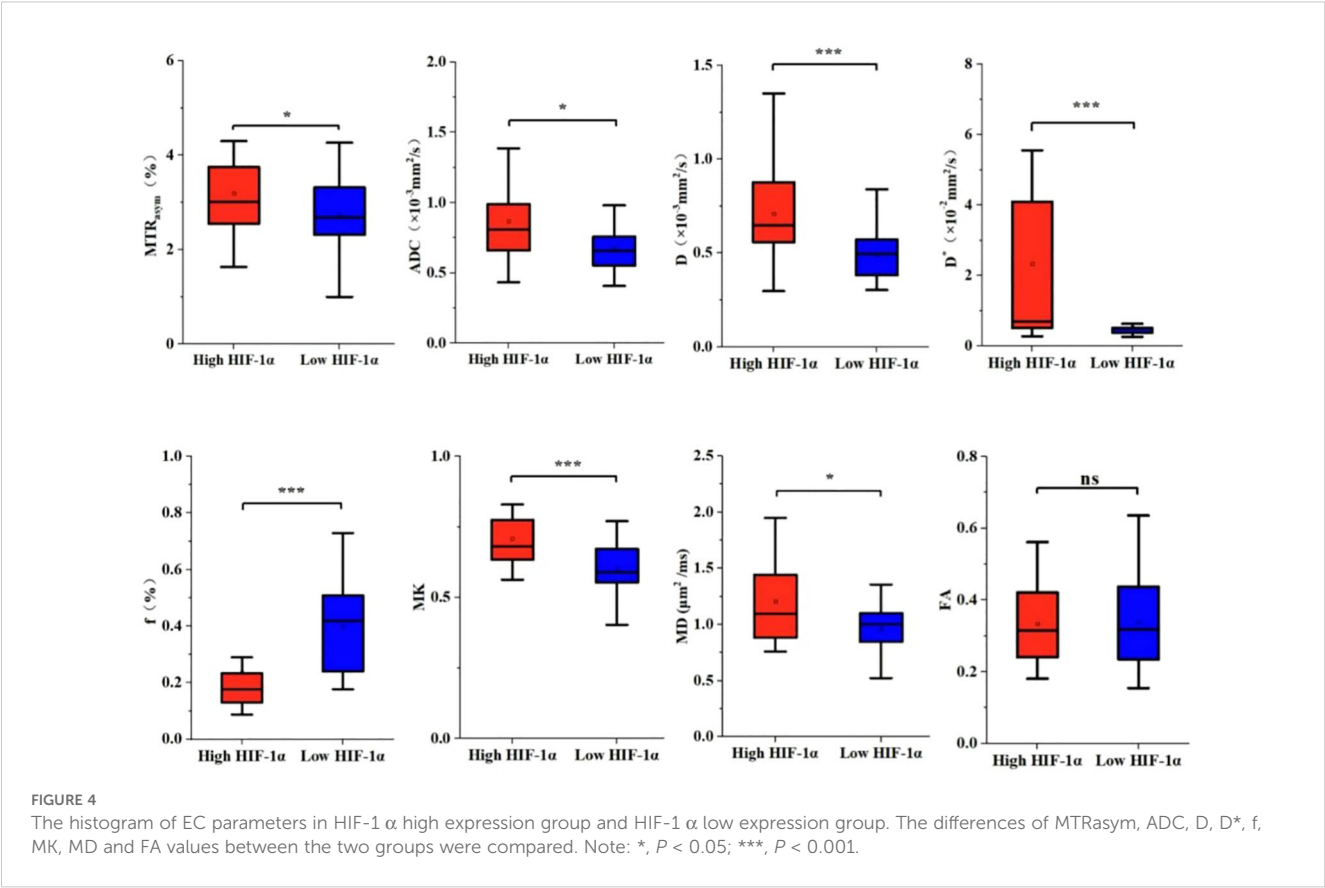
FIGURE 4

The histogram of EC parameters in HIF-1 α high expression group and HIF-1 α low expression group. The differences of MTRasym, ADC, D, D*, f, MK, MD and FA values between the two groups were compared. Note: *, $P < 0.05$; ***, $P < 0.001$.

TABLE 5 Univariate and multivariate analysis for identifying low HIF-1α expression and high HIF-1α expression patient groups.

Parameters	Univariate Analysis		Multivariate Analysis	
	OR (95%CI)	P	OR (95%CI)	P
Irregular vaginal bleeding	0.378(0.143 - 0.997)	0.049	0.545(0.053 - 5.594)	0.609
MTR$_{asym}$	1.007(1.001 - 1.013)	0.032	1.006(0.995 - 1.017)	0.303
ADC	1.034(1.010 - 1.059)	0.005	0.985(0.907 - 1.070)	0.726
D	1.061(1.025 - 1.098)	0.001	1.031(0.891 - 1.192)	0.683
D*	1.015(1.002 - 1.027)	0.026	1.012(0.996 - 1.027)	0.136
f	0.939(0.907 - 0.973)	<0.001	0.900(0.817 - 0.991)	0.032
MK	1.102(1.039 - 1.169)	0.001	1.161(1.035 - 1.301)	0.011
MD	1.028(1.006 - 1.050)	0.011	1.086(1.002 - 1.178)	0.046

The bold values in the tables indicate p-values < 0.05, denoting statistical significance.
OR, odds ratio; CI, confidence interval; MTRasym, Asymmetric magnetization transfer rate; ADC, Apparent diffusion coefficient; D, pure diffusion coefficient; D*, pseudo diffusion coefficient; f, perfusion fraction; MK, mean kurtosis; MD, mean diffusivity; FA, fractional anisotropy.

coefficient, reflecting the complexity of the tissue structure, while MK represents the average diffusion kurtosis, reflecting the overall diffusion level and diffusion resistance of water molecules.

Image analysis

Image analysis and data measurement were performed independently by three radiologists (TS F, MC J and LJ, with 10, 4 and 2 years of experience in uterine MR readings, respectively) who were blinded to the clinical and imaging data. The APTw and IVIM images were transferred to Intellispace Portal workstation, and the DKI images were transferred to GE AW4.6 workstation for post-processing. The specific measurement method is as follows: First, the maximum cross-sectional tumor on the conventional T$_2$WI and DWI image was located; Second, each parameter map were merged with the DWI images (b=800 s/mm^2) of the same layer to draw the regions of interest (ROIs) on the maximum cross-sectional tumor by using a freehand tool, which should include as many solid areas of the tumor as possible (Figures 2, 3). Every ROI was carefully positioned to avoid necrosis, hemorrhage, cystic degeneration, blood vessels, and partial volume effects on the edge of tumors. The mean value from the ROI for each parameter was recorded for further analysis.

Pathologic analysis

The paraffin blocks of endometrial cancer tissues submitted for examination in the pathology department of our hospital were

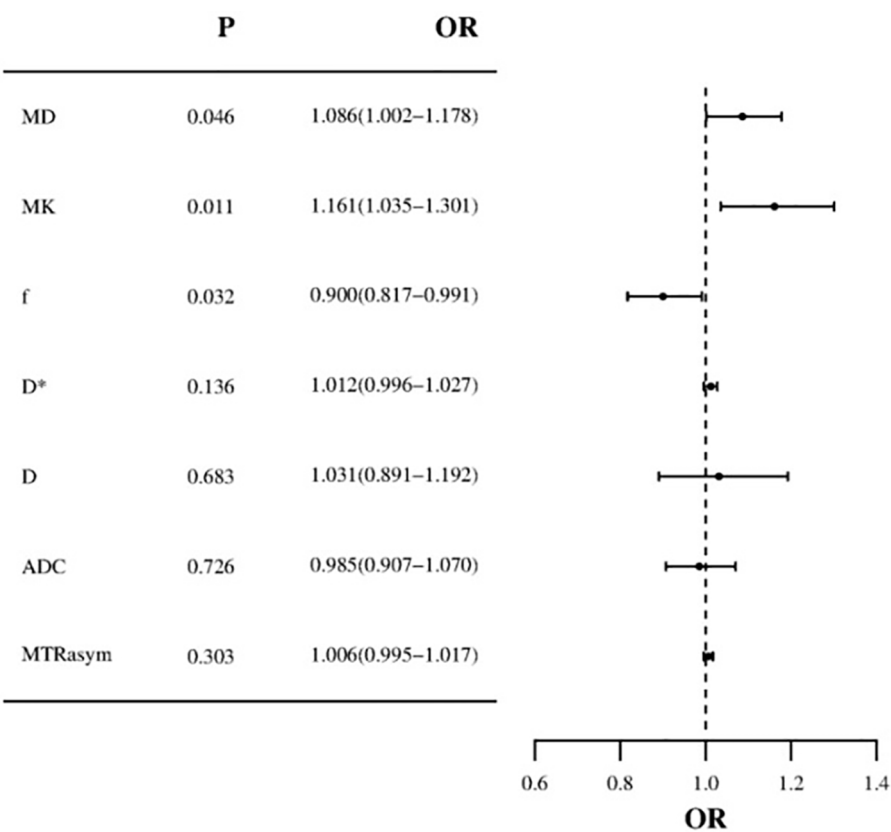|	P	OR
MD	0.046	1.086(1.002–1.178)
MK	0.011	1.161(1.035–1.301)
f	0.032	0.900(0.817–0.991)
D*	0.136	1.012(0.996–1.027)
D	0.683	1.031(0.891–1.192)
ADC	0.726	0.985(0.907–1.070)
MTRasym	0.303	1.006(0.995–1.017)

FIGURE 5
Forest plot of multivariate logistic regression (MD and MK values are risk factors for HIF-1α in EC, f value is protective factor for HIF-1α in EC).

collected retrospectively, and then 4 μm sections were made by a pathology technician with 10 years of pathological wax section experience, and sealed and preserved in a cool and dark environment. Then a graduate student with 3 years' experience of immunohistochemical experiment performed HIF-1α

immunohistochemical experiment in the pathology laboratory, and the staining was observed by two-step immunohistochemical method. The specific staining process included: baking, dewaxing, antigen repair, blocking endogenous peroxidase, first antibody incubation, second antibody incubation, Diaminobenzidine Horseradish
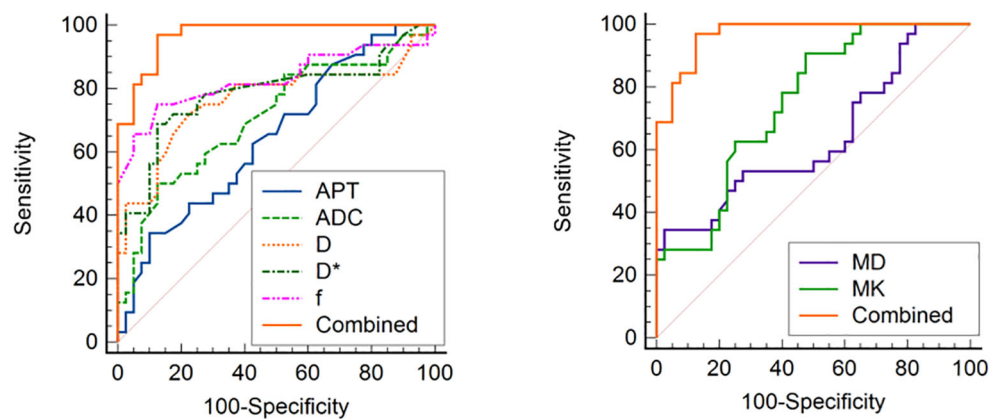
FIGURE 6
ROC curve analysis of the performance of each imaging parameter to evaluate the HIF-1α expression, AUCs of APT, ADC, D, D*, f, MD, MK, and Combined to evaluate the HIF-1α expression are 0.894 (0.740, 0.973), 0.746 (0.568, 0.879), 0.716 (0.528, 0.904), 0.920 (0.772, 0.984), 0.756 (0.578, 0.886), 0.973 (0.851–1.000), respectively.

TABLE 6 Predictive performance for identifying low HIF-1α expression and high HIF-1α expression EC.

Parameters	AUC (95% CI)	P	Cutoff	Sensitivity (%)	Specificity (%)	DeLong test	
MTR$_{asym}$	0.646 (0.519 – 0.774)	0.034	3.515	65.60	90.00	Z =4.940	<0.001
ADC	0.709 (0.586 – 0.832)	0.002	0.815	50.00	87.50	Z=4.161	<0.001
D	0.763 (0.640 – 0.885)	<0.001	0.575	71.90	77.50	Z=3.335	<0.001
D*	0.784 (0.669 – 0.900)	<0.001	0.585	68.80	87.50	Z=3.300	0.001
f	0.828 (0.720 – 0.935)	<0.001	0.225	87.50	75.00	Z=2.608	0.009
MK	0.750 (0.639 - 0.860)	<0.001	0.593	90.60	52.50	Z=4.033	<0.001
MD	0.637 (0.505 - 0.769)	0.047	1.227	44.50	97.50	Z=4.976	<0.001
Combined (a.u.)	0.970 (0.938 - 1.000)	<0.001	0.251	96.90	85.00	NA	NA

MTRasym, asymmetric magnetization transfer rater; ADC, apparent diffusion coefficient; D, true diffusion; D*, pseudo diffusion; f, perfusion fraction; MK, mean kurtosis; MD, mean diffusivity; OR, odds ratio; CI, confidence interval; a.u., arbitrary unit; NA, not available.
The bold values in the tables indicate p-values < 0.05, denoting statistical significance.

Peroxidase Color Development Kit working solution coloration, re-staining and dehydration sealing. The staining results were evaluated by two doctors with 3 and 4 years' pathology experience respectively without knowing the clinical and imaging information. When results of the two assessments were inconsistent, they discussed and agreed with another pathologist with 10 years of experience. Among them, HIF-1α is mainly expressed in the nucleus, and observed under a high-power microscope, 3 visual fields are randomly selected from each tissue section, and then the expression level is judged comprehensively according to the percentage of positive cells and staining intensity: the total positive score is 0 (less than 1%), 1 (1% ~ 10%), 2 (11% ~ 50%), 3 (51% ~ 80%), and 4 (> 80%). The staining intensity scores were 0 (no staining), 1 (light yellow), 2 (dark yellow), and 3 (dark brown). The EC was defined as high expression group when HIF-1 α positive cells were more than 50% and staining intensity ≥ 2 points, otherwise they were defined as low expression group (Figures 2, 3).

Statistical analysis

Statistical analysis was performed using SPSS 27.0 software (Chicago, IL, USA) and MedCalc15.2.2 software (MedC Software, Ostend, Belgium). The inter-class correlation coefficient (ICC) was employed to assess the agreement among the measurements provided by three observers. ICC values of 0.40 and 0.75 were utilized as thresholds for categorizing the consistency levels as low, medium, and high. The mean of the measurements obtained from the three observers was utilized for further analysis. The Kolmogorov-Smirnov test was conducted to evaluate the normality of the measurement data.

The data adhering to a normal distribution were presented as mean ± standard deviation and analyzed using an independent sample t-test for group comparisons. Data not conforming to a normal distribution were represented as median (25th percentile, 75th percentile) and analyzed using the Mann-Whitney U test. Categorical data were expressed as frequencies and percentages, and group comparisons were conducted using the Chi-square test or Fisher's exact test. Receiver operating characteristic (ROC) curve analysis was utilized to assess the predictive value of statistically significant parameters and their combinations in predicting low and high HIF-1α expression in EC. Binary logistic regression was employed to determine the predictive value of EC HIF-1α expression status in conjunction with independent risk factors. The area under the curve (AUC) was compared using the Delong test. A P-value less than 0.05 was considered statistically significant.

Result

Patient characteristics

Of the 72 EC patients finally enrolled, 32 (44.44%) were in the high HIF-1α expression group, and 40 (55.56%) were in the low HIF-1α expression group. Based on the pathological analysis, there were no statistically significant differences observed between the two groups in terms of age, differentiation degree, menopausal state, FIGO stage, DMI, LVSI, LNM, and pathological type. However, a significant difference was found between the two groups in presence of irregular vaginal bleeding (P=0.040), as presented in Table 1.

Agreement on imaging parameters among the three observers

The three observers had high consistency on measurements of the MTR_{asym}, ADC, D, D*, f, MK, FA, and MD values with the ICCs higher than 0.75, as shown in Table 3.

Comparison of imaging parameters between high and low HIF-1α expression groups

The imaging parameters for high and low HIF-1α expression groups are presented in Table 4. MTR_{asym}, ADC, D, D*, MK and MD values were significantly higher in high HIF-1α expression than those in low HIF-1α expression groups, whereas f value was significantly lower in high HIF-1α expression than in low HIF-1α expression groups (Figure 4).

Regression analyses

Based on the comprehensive clinicopathological data and various quantitative parameters with P values below 0.1 in the comparison between the two groups, multiple linear regression analysis was conducted to assess covariance interference. It is found that except for D (11.368, excluded in the multiple linear regression analysis), the variance expansion factors (VIF) of other parameters were all less than 10 (MTR_{asym}=1.104, ADC=6.654, D*=2.472, f=1.906, MK=1.135, and MD=1.251). Univariate analysis showed that irregular vaginal bleeding, MTR_{asym}, ADC, D, D*, f, MK and MD were all helpful to evaluate the expression of HIF-1α in EC, but multivariate analysis showed that only f, MK and MD were independent predictors of HIF-1α expression in EC (Table 5, Figure 5).

Ability of the imaging parameters to discriminate high HIF-1α expression from low HIF-1α expression groups

ROC curves for APTw and multiple model DWI parameters and their combinations to discriminate high HIF-1α expression from low HIF-1α expression are shown in Figure 6. MTR_{asym}, ADC, D, D*and f values commonly had good specificity (90.00%, 87.50%, 77.50%, 87.50% and 75.00%), while moderate sensitivity (65.60%, 50.00%, 71.90%, 68.80% and 87.50%). Combination of the above parameters showed significantly improved diagnostic performance with excellent sensitivity (96.90%) and specificity (85.00%) (Table 6). The ROCs for each parameters and their combination are shown in Figure 6.

Correlation analysis between independent factors and HIF-1α expression

Spearman rank correlation analysis showed that there was an inverse correlation between f and HIF-1α expression level (rho = -0.565; P < 0.001). MK and MD showed positive correlations with the HIF-1α expression level (rho = 0.430, 0.316; both P < 0.001).

Discussion

The major finding of this work was that multimodal quantitative MRI parameters, by APTw, DWI, DKI and IVIM, can be used to assess the HIF-1α expression in EC. We found that APT, ADC, D, D*, MK and MD values were significantly higher in high HIF-1α expression than in low HIF-1α expression groups, whereas f value was significantly lower in high HIF-1α expression than in low HIF-1α expression groups, meanwhile, the f value, MK value, and MD value are independent risk factors for predicting HIF-1α expression in EC. There was an inverse correlation between f and HIF-1α expression level, and there were positive correlations of MK value, and MD value with the HIF-1α expression level. The combination of different imaging parameters showed a significantly improved diagnostic efficacy in differentiation of HIF-1α expression in EC.

APTw imaging can be used to evaluate changes of intracellular protein concentration and tissue pH value with advantages of non-invasive and quantitative analysis (38–40). In this study, the MTR_{asym} of HIF-1 α high expression group was higher than that of low expression group, and the difference was statistically significant. The reason may be that the expression of HIF-1 α can regulate the metabolism and proliferation of local tumor (15), the number of cells in the local tumor increases and the metabolism is exuberant, which leads to the increase of local mobile proteins or peptides and the increase of MTR_{asym} in the group with high expression of HIF-1 α. Nuclear atypia, which induce the interaction between macromolecules and hydrophobic cell membrane and promote the release of proteins and peptides, may be another factor in the increase of MTR_{asym} in malignant tumors (41, 42). Although there was no difference in the pathological indexes of the degree of tumor differentiation, depth of myometrial invasion and tumor stage between the two groups (due to the small sample size and bias), previous studies (43, 44) showed that the tumors with higher expression of HIF-1α had lower tissue differentiation, deeper myometrial invasion, higher probability of lymph node metastasis and higher malignant degree of tumor. In addition, pH value is also one of the factors affecting MTR_{asym} (45, 46). Tumor with higher expression of HIF-1α can be associated with serious local hypoxia (47), where the tumor is mainly anaerobic metabolism, leading to increased production of local lactic acid and reduced pH value. However, the higher expression of HIF-1α can also induce the expression of vascular endothelial growth factor (VEGF) and other genes, which leads to the increase of tumor angiogenesis and local tumor microcirculation perfusion (48), and dilutes tumor local acidity to some extent. It may lead to the relative increase of pH value,

which in turn leads to the increase of MTR$_{asym}$ value. However, as mentioned above, the high expression of HIF-1α increases the expression of VEGF and other genes (49), tumor neovascularization, local tumor microcirculation perfusion, and dilutes tumor local acidity to some extent. It may lead to the relative increase of pH value, which in turn leads to the increase of MTR$_{asym}$ value. At the same time, the perfusion parameter D* of the group with high expression of HIF-1α was higher than that of the group with low expression of HIF-1α, which further indicated that the perfusion of local microcirculation was increased in the group with high expression of HIF-1α. Compared with the results by Li et al. (42), the MTR$_{asym}$ and D* values of cervical squamous cell carcinoma in poorly differentiated group were higher than those in well differentiated group, which also verified the hypothesis of the relationship between the change of MTR$_{asym}$ value caused by the change of pH value and the perfusion parameter D* value of IVIM microcirculation.

The parameter D from the double exponential IVIM model (50) reflect the diffusion movement of water molecules without microperfusion (51), D* represents the diffusion effect caused by blood perfusion and reflects the perfusion of microcirculation in capillaries (52), and f reflects the percentage of the volume of water molecules in blood vessels to the volume of water molecules in the whole voxel (35). DKI is based on non-Gaussian distribution, which truly reflects that the movement of water molecules in living tissues is limited by tissue microstructure (53). The parameter MK by DKI can reflect the complexity of tissue structure, while MD value can reflect the overall diffusion level and diffusion resistance of water molecules (54). In this study, the parameters reflecting the diffusion of water molecules in EC (ADC, D and MD) were higher in the high HIF-1α expression than in the low expression group, which may be due to that the higher expression of HIF-1α may results in the increased proliferation of local tumor cells (15), and thus reduced extracellular space in EC. In addition, the MK value of the parameter reflecting the complexity of tumor tissue was also higher in the high HIF-1α expression than that in the low expression groups, which was related to the fact that the expression of HIF-1α could regulate the proliferation and epithelial mesenchymal transition of tumor cells, resulting in the exuberant proliferation of tumor local cells, the increase of epithelial stromal transition and the complexity of tumor local structure (15, 16). At the same time (55), the expression of HIF-1α can also regulate the apoptosis of tumor cells, which complicates the structural components of tumor tissue, which is another reason for the increase of MK in EC patients with high expression of HIF-1α. The D* and f values were higher in the group with high expression of HIF-1α, because the expression of HIF-1α could induce the expression of VEGF and other genes (49), which increased tumor angiogenesis and local microcirculation perfusion, which was consistent with the results of previous studies on IVIM to evaluate the expression level of HIF-1α in cervical cancer (35). However, in this study, the f value of EC in the high expression group of HIF-1α was lower than that in the low expression group EC. The reason may be that the value of f is not only related to microvessel density and blood flow velocity, but can also be related to the overall motion state of water molecules in tissue, vascular wall pressure and the b value setting in IVIM scan (51, 56–58). Pang et al. (59) found

that when the b value varies from 0 to 700 s/mm^2, the f value increases, while when the b value exceeds 700 s/mm^2, the f value decreases. In this study, the b value of IVIM is between 0 and 2000 s/mm^2, which makes the change trend of f value decrease with the increase of b. The high expression of HIF-1α associated with increased proliferation of tumor cells can results in the higher pressure on tumor neovascularization wall, which may slow down the blood flow velocity of local tumor microcirculation and lead to the reduced f value. Multivariate analysis showed that f value was a protective factor for the high expression of EC HIF-1α, and there was a negative correlation between f value and HIF-1α expression, which further indicated that the higher the f value, the weaker the invasive biological behavior of tumor cells and the lower the malignant degree of tumor, so the lower expression level of HIF-1α.

The shortcomings of this study are as follows: firstly, the sample size of this study is small, which needs to be further studied by increasing the sample size; secondly, the quantitative parameter measurement of this study avoids bleeding and necrosis, and does not outline the tumor globally, and some heterogeneity information may be omitted, which need to be studied in the future, such as texture analysis. The image quality of APTw, IVIM and DKI maps can be affected by respiratory movement, which needs to be optimized by respiratory trigger.

In summary, the quantitative parameters based on APTw and multi-model diffusion imaging can effectively evaluate the expression of EC HIF-1α, which has a certain prospect of clinical applications.

Data availability statement

The datasets presented in this article are not readily available because it contains sensitive information that cannot be shared publicly due to privacy and legal restrictions. Additionally, the datasets are part of an ongoing study, and making them publicly accessible at this stage could compromise the integrity of the research. We are willing to consider reasonable requests for access on a case-by-case basis, subject to appropriate approvals and agreements. Requests to access the datasets should be directed to JL, junjun54586@163.com.

Ethics statement

The studies involving humans were approved by Dalian Medical Science Research Program Project. The studies were conducted in accordance with the local legislation and institutional requirements. The participants provided their written informed consent to participate in this study. The Ethics Committee approved this retrospective study and waived the requirement of informed consent (PJ-KS-KY-2023-265).

Author contributions

JL: Writing – original draft, Conceptualization, Data curation, Formal Analysis, Investigation, Methodology, Software, Validation. CM: Writing – review & editing. ST: Writing – review & editing. AL: Writing – review

& editing. QLS: Writing – review & editing. NW: Writing – review & editing. QWS: Writing – review & editing. LL: Writing – review & editing. PS: Writing – review & editing. JW: Writing – review & editing.

Funding

Conflict of interest

Authors LL, PS and JW were employed by Philips Health Technology (China) Co., Ltd.

The remaining authors declare that the research was conducted in the absence of any commercial or financial relationships that could be construed as a potential conflict of interest.

The author(s) declared that they were an editorial board member of Frontiers, at the time of submission. This had no impact on the peer review process and the final decision.

Generative AI statement

The author(s) declare that no Generative AI was used in the creation of this manuscript.

Publisher's note

All claims expressed in this article are solely those of the authors and do not necessarily represent those of their affiliated organizations, or those of the publisher, the editors and the reviewers. Any product that may be evaluated in this article, or claim that may be made by its manufacturer, is not guaranteed or endorsed by the publisher.

References

1. Sung H, Ferlay J, Siegel RL, Laversanne M, Soerjomataram I, Jemal A, et al. Global cancer statistics 2020: GLOBOCAN estimates of incidence and mortality worldwide for 36 cancers in 185 countries. *CA Cancer J Clin*. (2021) 71:209–49. doi: 10.3322/caac.21660

2. Makker V, MacKay H, Ray-Coquard I, Levine DA, Westin SN, Aoki D, et al. Endometrial cancer. *Nat Rev Dis Prime*. (2021) 7:88. doi: 10.1038/s41572-021-00324-8

3. Siegel RL, Miller KD, Fuchs HE, Jemal A. Cancer statistics, 2022. *CA Cancer J Clin*. (2022) 72:7–33. doi: 10.3322/caac.21708

4. Degez M, Caillon H, Chauviré-Drouard A, Leroy M, Lair D, Winer N, et al. Endometrial cancer: A systematic review of HE4, REM and REM-B. *Clin Chim Acta*. (2021) 515:27–36. doi: 10.1016/j.cca.2020.12.029

5. D'Oria O, Giannini A, Besharat AR, Caserta D. Management of endometrial cancer: molecular identikit and tailored therapeutic approach. *Clin Exp Obstet Gynecol*. (2023) 50:210. doi: 10.31083/j.ceog5010210

6. Singh N, Hirschowitz L, Zaino R, Alvarado-Cabrero I, Duggan MA, Ali-Fehmi R, et al. Pathologic prognostic factors in endometrial carcinoma (Other than tumor type and grade). *Int J Gynecol Pathol*. (2019) 38 Suppl 1:S93–S113. doi: 10.1097/PGP.0000000000000524

7. Harris KL, Maurer KA, Jarboe E, Werner TL, Gaffney D. LVSI positive and NX in early endometrial cancer: Surgical restaging (and no further treatment if N0), or adjuvant ERT? *Gynecol Oncol*. (2020) 156:243–50. doi: 10.1016/j.ygyno.2019.09.016

8. Koppikar S, Oaknin A, Babu KG, Lorusso D, Gupta S, Wu LY, et al. Pan-Asian adapted ESMO Clinical Practice Guidelines for the diagnosis, treatment and follow-up of patients with endometrial cancer. *ESMO Open*. (2023) 8:100774. doi: 10.1016/j.esmoop.2022.100774

9. Guo J, Fan J, Zhang Y, Li M, Jin Z, Shang Y, et al. Progesterone inhibits endometrial cancer growth by inhibiting glutamine metabolism through ASCT2. *Biosci Rep*. (2024) 44:BSR20232035. doi: 10.1042/BSR20232035

10. Shang X, Su H, Chen X, Wang Y, Wan X, Zhang Y, et al. Low-dose lenvatinib and anti-programmed cell death protein-1 combination therapy in patients with heavily pre-treated recurrent ovarian and endometrial cancer: a pilot study. *Int J Gynecol Cancer*. (2024) 34:1203–10. doi: 10.1136/ijgc-2024-005331

11. Salinas-Vera YM, Gallardo-Rincón D, Ruíz-García E, Silva-Cázares MB, de-la-Peña-Cruz CS, López-Camarillo C. The role of hypoxia in endometrial cancer. *Curr Pharm Biotechnol*. (2022) 23:221–34. doi: 10.2174/1389201022666210224130022

12. Zhu P, Shen L, Ren Q, Zeng Q, He X. Prognostic and clinicopathological significance of hypoxia-inducible factor-1α in endometrial cancer: A meta-analysis. *Front Oncol*. (2020) 10:587420. doi: 10.3389/fonc.2020.587420

13. Ellingsen C, Andersen LM, Galappathi K, Rofstad EK. Hypoxia biomarkers in squamous cell carcinoma of the uterine cervix. *BMC Cancer*. (2015) 15:805. doi: 10.1186/s12885-015-1828-2

14. Nishi H, Sasaki T, Nagamitsu Y, Terauchi F, Nagai T, Nagao T, et al. Hypoxia inducible factor-1 mediates upregulation of urokinase-type plasminogen activator receptor gene transcription during hypoxia in cervical cancer cells. *Oncol Rep*. (2016) 35:992–8. doi: 10.3892/or.2015.4449

15. Lin CS, Liu TC, Lee MT, Yang SF, Tsao TC. Independent prognostic value of hypoxia-inducible factor 1-alpha expression in small cell lung cancer. *Int J Med Sci*. (2017) 14:785–90. doi: 10.7150/ijms.19512

16. Liu X, Zhang X, Peng Z, Li C, Wang Z, Wang C, et al. Deubiquitylase OTUD6B governs pVHL stability in an enzyme-independent manner and suppresses hepatocellular carcinoma metastasis. *Adv Sci (Weinh)*. (2020) 7:1902040. doi: 10.1002/advs.201902040

17. Jiang L, Shi S, Shi Q, Zhang H, Hu R, Wang M. Similarity in the functions of HIF-1α and HIF-2α proteins in cervical cancer cells. *Oncol Lett*. (2017) 14:5643–51. doi: 10.3892/ol.2017.6837

18. Bosco MC, D'Orazi G, Del Bufalo D. Targeting hypoxia in tumor: a new promising therapeutic strategy. *J Exp Clin Cancer Res*. (2020) 39:8. doi: 10.1186/s13046-019-1517-0

19. Lee JW, Bae SH, Jeong JW, Kim SH, Kim KW. Hypoxia-inducible factor (HIF-1) alpha: its protein stability and biological functions. *Exp Mol Med*. (2004) 36:1–12. doi: 10.1038/emm.2004.1

20. Gao A, Zhang M, Zhu SQ, Zou S, Chen H, Li X, et al. DNA polymerase iota promotes EMT and metastasis of esophageal squamous cell carcinoma by interacting with USP7 to stabilize HIF-1α. *Cell Death Dis*. (2024) 15:171. doi: 10.1038/s41419-024-06552-6

21. Yin CL, Ma YJ. The regulatory mechanism of hypoxia-inducible factor 1 and its clinical significance. *Curr Mol Pharmacol*. (2024):e18761429266116. doi: 10.2174/0118761429266116231123160809

22. Musleh Ud Din S, Streit SG, Huynh BT, Hana C, Abraham AN, Hussein A. Therapeutic targeting of hypoxia-inducible factors in cancer. *Int J Mol Sci*. (2024) 25:2060. doi: 10.3390/ijms25042060

23. Cantelmo AR, Conradi LC, Brajic A, Goveia J, Kalucka J, Pircher A, et al. Inhibition of the glycolytic activator PFKFB3 in endothelium induces tumor vessel normalization, impairs metastasis, and improves chemotherapy. *Cancer Cell*. (2016) 30:968–85. doi: 10.1016/j.ccell.2016.10.006

24. Liao ZH, Zhu HQ, Chen YY, Chen RL, Fu LX, Li L, et al. The epigallocatechin gallate derivative Y6 inhibits human hepatocellular carcinoma by inhibiting angiogenesis in MAPK/ERK1/2 and PI3K/AKT/HIF-1α/VEGF dependent pathways. *J Ethnopharmacol*. (2020) 259:112852. doi: 10.1016/j.jep.2020.112852

25. Cheng CW, Liu YF, Liao WL, Chen PM, Hung YT, Lee HJ, et al. miR-622 Increases miR-30a Expression through Inhibition of Hypoxia-Inducible Factor 1α to Improve Metastasis and Chemoresistance in Human Invasive Breast Cancer Cells. *Cancers (Basel)*. (2024) 16:657. doi: 10.3390/cancers16030657

26. Bettoni F, Masotti C, Habr-Gama A, Correa BR, Gama-Rodrigues J, Vianna MR, et al. Intratumoral Genetic Heterogeneity in Rectal Cancer: Are Single Biopsies representative of the entirety of the tumor? *Ann Surg*. (2017) 265:e4–6. doi: 10.1097/SLA.0000000000001937

27. Bogani G, Chiappa V, Lopez S, Salvatore C, Interlenghi M, D'Oria O, et al. Radiomics and molecular classification in endometrial cancer (The ROME study): A step forward to a simplified precision medicine. *Healthc (Basel)*. (2022) 10:2464. doi: 10.3390/healthcare10122464

28. Di Donato V, Kontopantelis E, Cuccu I, Sgamba L, Golia D'Augè T, Pernazza A, et al. Magnetic resonance imaging-radiomics in endometrial cancer: a systematic review and meta-analysis. *Int J Gynecol Cancer*. (2023) 33:1070–6. doi: 10.1136/ijgc-2023-004313

29. Casolino R, Beer PA, Chakravarty D, Davis MB, Malapelle U, Mazzarella L, et al. Interpreting and integrating genomic tests results in clinical cancer care: Overview and practical guidance. *CA Cancer J Clin*. (2024) 74:264–85. doi: 10.3322/caac.21825

30. Liu Y, Gu Y, Yuan W, Zhou X, Qiu X, Kong M, et al. Quantitative mapping of liver hypoxia in living mice using time-resolved wide-field phosphorescence lifetime imaging. *Adv Sci (Weinh)*. (2020) 7:1902929. doi: 10.1002/advs.201902929

31. Salem A, Little RA, Latif A, Featherstone AK, Babur M, Peset I, et al. Oxygen-enhanced MRI is feasible, repeatable, and detects radiotherapy-induced change in hypoxia in xenograft models and in patients with non-small cell lung cancer. *Clin Cancer Res*. (2019) 25:3818–29. doi: 10.1158/1078-0432.CCR-18-3932

32. Bakke KM, Meltzer S, Grøvik E, Negård A, Holmedal SH, Gjesdal KI, et al. Sex differences and tumor blood flow from dynamic susceptibility contrast MRI are associated with treatment response and long-term survival in rectal cancer. *Radiology*. (2020) 297:352–60. doi: 10.1148/radiol.2020200287

33. Mahajan A, Engineer R, Chopra S, Mahanshetty U, Juvekar SL, Shrivastava SK, et al. Role of 3T multiparametric-MRI with BOLD hypoxia imaging for diagnosis and post therapy response evaluation of postoperative recurrent cervical cancers. *Eur J Radiol Open*. (2015) 3:22–30. doi: 10.1016/j.ejro.2015.11.003

34. Wegner CS, Hauge A, Simonsen TG, Gaustad JV, Andersen LMK, Rofstad EK. DCE-MRI of sunitinib-induced changes in tumor microvasculature and hypoxia: A study of pancreatic ductal adenocarcinoma xenografts. *Neoplasia*. (2018) 20:734–44. doi: 10.1016/j.neo.2018.05.006

35. Li X, Wu S, Li D, Yu T, Zhu H, Song Y, et al. Intravoxel incoherent motion combined with dynamic contrast-enhanced perfusion MRI of early cervical carcinoma: correlations between multimodal parameters and HIF-1α Expression. *J Magn Reson Imag*. (2019) 50:918–29. doi: 10.1002/jmri.26604

36. Le Bihan D, Breton E, Lallemand D, Aubin ML, Vignaud J, Laval-Jeantet M. Separation of diffusion and perfusion in intravoxel incoherent motion MR imaging. *Radiology*. (1988) 168:497–505. doi: 10.1148/radiology.168.2.3393671

37. Yang ZL, Li Y, Zhan CA, Hu YQ, Guo YH, Xia LM, et al. Evaluation of suspicious breast lesions with diffusion kurtosis MR imaging and connection with prognostic factors. *Eur J Radiol*. (2021) 145:110014. doi: 10.1016/j.ejrad.2021.110014

38. Zhou J, Heo HY, Knutsson L, van Zijl PCM, Jiang S. APT-weighted MRI: Techniques, current neuro applications, and challenging issues. *J Magn Reson Imag*. (2019) 50:347–64. doi: 10.1002/jmri.26645

39. Zhou J, Payen JF, Wilson DA, Traystman RJ, van Zijl PC. Using the amide proton signals of intracellular proteins and peptides to detect pH effects in MRI. *Nat Med*. (2003) 9:1085–90. doi: 10.1038/nm907

40. Zhou J, Lal B, Wilson DA, Laterra J, van Zijl PC. Amide proton transfer (APT) contrast for imaging of brain tumors. *Magn Reson Med*. (2003) 50:1120–6. doi: 10.1002/mrm.10651

41. Schurink NW, Lambregts DMJ, Beets-Tan RGH. Diffusion-weighted imaging in rectal cancer: current applications and future perspectives. *Br J Radiol*. (2019) 92:20180655. doi: 10.1259/bjr.20180655

42. Li B, Sun H, Zhang S, Wang X, Guo Q. The utility of APT and IVIM in the diagnosis and differentiation of squamous cell carcinoma of the cervix: A pilot study. *Magn Reson Imag*. (2019) 63:105–13. doi: 10.1016/j.mri.2019.08.020

43. Eckert AW, Horter S, Bethmann D, Kotrba J, Kaune T, Rot S, et al. Investigation of the prognostic role of carbonic anhydrase 9 (CAIX) of the cellular mRNA/protein level or soluble CAIX protein in patients with oral squamous cell carcinoma. *Int J Mol Sci*. (2019) 20:375. doi: 10.3390/ijms20020375

44. Zhang J, Wu Y, Lin YH, Guo S, Ning PF, Zheng ZC, et al. Prognostic value of hypoxia-inducible factor-1 alpha and prolyl 4-hydroxylase beta polypeptide overexpression in gastric cancer. *World J Gastroenterol*. (2018) 24:2381–91. doi: 10.3748/wjg.v24.i22.2381

45. Jokivarsi KT, Gröhn HI, Gröhn OH, Kauppinen RA. Proton transfer ratio, lactate, and intracellular pH in acute cerebral ischemia. *Magn Reson Med*. (2007) 57:647–53. doi: 10.1002/mrm.21181

46. Ray KJ, Simard MA, Larkin JR, Coates J, Kinchesh P, Smart SC, et al. Tumor pH and protein concentration contribute to the signal of amide proton transfer magnetic resonance imaging. *Cancer Res*. (2019) 79:1343–52. doi: 10.1158/0008-5472.CAN-18-2168

47. Chen H, Chen J, Yuan H, Li X, Li W. Hypoxia-inducible factor-1α: A critical target for inhibiting the metastasis of hepatocellular carcinoma. *Oncol Lett*. (2022) 24:284. doi: 10.3892/ol.2022.13404

48. Zhang EY, Gao B, Shi HL, Huang LF, Yang L, Wu XJ, et al. 20(S)-Protopanaxadiol enhances angiogenesis via HIF-1α-mediated VEGF secretion by activating p70S6 kinase and benefits wound healing in genetically diabetic mice. *Exp Mol Med*. (2017) 49:e387. doi: 10.1038/emm.2017.151

49. Kim MH, Jeong YJ, Cho HJ, Hoe HS, Park KK, Park YY, et al. Delphinidin inhibits angiogenesis through the suppression of HIF-1α and VEGF expression in A549 lung cancer cells. *Oncol Rep*. (2017) 37:777–84. doi: 10.3892/or.2016.5296

50. Pu J, Liang Y, He Q, Shao JW, Zhou MJ, Xiang ST, et al. Correlation between IVIM-DWI parameters and pathological classification of idiopathic orbital inflammatory pseudotumors: A preliminary study. *Front Oncol*. (2022) 12:809430. doi: 10.3389/fonc.2022.809430

51. Sauer M, Klene C, Kaul M, Quitzke A, Avanesov M, Behzadi C, et al. Preoperative evaluation of pelvine lymph node metastasis in high risk prostate cancer with intravoxel incoherent motion (IVIM) MRI. *Eur J Radiol*. (2018) 107:1–6. doi: 10.1016/j.ejrad.2018.07.029

52. Gao F, Shi B, Wang P, Wang C, Fang X, Dong J, et al. The value of intravoxel incoherent motion diffusion-weighted magnetic resonance imaging combined with texture analysis of evaluating the extramural vascular invasion in rectal adenocarcinoma. *Front Oncol*. (2022) 12:813138. doi: 10.3389/fonc.2022.813138

53. Zhang D, Geng X, Suo S, Zhuang Z, Gu Y, Hua J. The predictive value of DKI in breast cancer: Does tumour subtype affect pathological response evaluations? *Magn Reson Imag*. (2021) 85:28–34. doi: 10.1016/j.mri.2021.10.013

54. Di Paola V, Perillo F, Gui B, Russo L, Pierconti F, Fiorentino V, et al. Detection of parametrial invasion in women with uterine cervical cancer using diffusion tensor imaging at 1.5T MRI. *Diagn Interv Imag*. (2022) 103:472–8. doi: 10.1016/j.diii.2022.05.005

55. Albadari N, Deng S, Li W. The transcriptional factors HIF-1 and HIF-2 and their novel inhibitors in cancer therapy. *Expert Opin Drug Discov*. (2019) 14:667–82. doi: 10.1080/17460441.2019.1613370

56. Matsuo K, Shimada M, Saito T, Takehara K, Tokunaga H, Watanabe Y, et al. Risk stratification models for para-aortic lymph node metastasis and recurrence in stage IB-IIB cervical cancer. *J Gynecol Oncol*. (2018) 29:e11. doi: 10.3802/jgo.2018.29.e11

57. Zheng W, Chen K, Peng C, Yin SH, Pan YY, Liu M, et al. Contrast-enhanced ultrasonography vs MRI for evaluation of local invasion by cervical cancer. *Br J Radiol*. (2018) 91:20170858. doi: 10.1259/bjr.20170858

58. Fu F, Meng N, Huang Z, Sun J, Wang X, Shang J, et al. Identification of histological features of endometrioid adenocarcinoma based on amide proton transfer-weighted imaging and multimodel diffusion-weighted imaging. *Quant Imaging Med Surg*. (2022) 12:1311–23. doi: 10.21037/qims-21-189

59. Pang Y, Turkbey B, Bernardo M, Kruecker J, Kadoury S, Merino MJ, et al. Intravoxel incoherent motion MR imaging for prostate cancer: an evaluation of perfusion fraction and diffusion coefficient derived from different b-value combinations. *Magn Reson Med*. (2013) 69:553–62. doi: 10.1002/mrm.24277